ARTICLES

Insight into the 2004 Sumatra–Andaman earthquake from GPS measurements in southeast Asia

C. Vigny[1], W. J. F. Simons[2], S. Abu[3], Ronnachai Bamphenyu[4], Chalermchon Satirapod[5], Nithiwatthn Choosakul[6], C. Subarya[7], A. Socquet[2]†, K. Omar[8], H. Z. Abidin[9] & B. A. C. Ambrosius[2]

Data collected at ~60 Global Positioning System (GPS) sites in southeast Asia show the crustal deformation caused by the 26 December 2004 Sumatra–Andaman earthquake at an unprecedented large scale. Small but significant co-seismic jumps are clearly detected more than 3,000 km from the earthquake epicentre. The nearest sites, still more than 400 km away, show displacements of 10 cm or more. Here we show that the rupture plane for this earthquake must have been at least 1,000 km long and that non-homogeneous slip is required to fit the large displacement gradients revealed by the GPS measurements. Our kinematic analysis of the GPS recordings indicates that the centroid of released deformation is located at least 200 km north of the seismological epicentre. It also provides evidence that the rupture propagated northward sufficiently fast for stations in northern Thailand to have reached their final positions less than 10 min after the earthquake, hence ruling out the hypothesis of a silent slow aseismic rupture.

The 26 December 2004 Sumatra–Andaman megathrust earthquake is associated with the continuing subduction process along the Sumatran trench. However, in this particular region, the subducting plate is neither entirely Australia nor entirely India. Therefore it is quite difficult to determine the exact relative motion on the subduction zone. According to the latest geodetic determination of plate tectonics in southeast Asia, the relative motion between Australia and Sundaland is 5 ± 0.3 cm yr^{-1} oriented 8 ± 2°N at the northern tip of Sumatra[1,2]. Relative to the Indian plate, the motion has a slightly different azimuth (20°N) and a lower velocity of 4 cm yr^{-1} (ref. 3). Previous GPS measurements in this area showed accumulation of elastic deformation in the overriding plate (Sundaland) owing to the locking of the subduction interface[4]. Dip angle and precise locking depths were difficult to estimate accurately, but the extent of residual deformation in the Malaysian peninsula and southern Thailand pointed towards a very large coupling zone. The 26 December 2004 earthquake corresponds to the elastic rebound of this large region. From initial seismological data and tsunami observations it was not clear whether the seismic rupture was confined to a length of ~450 km or continued 500 km to the north in either a seismic mode or in a slow (and 'silent') mode. Recent, new GPS data shared in the framework of the EU-ASEAN 'South-East Asia: Mastering Environmental Research Using Geodetic Space Techniques' (SEAMERGES) project enable us to quantify the widespread surface deformation and hence to determine the size of the rupture.

GPS-observed co-seismic deformation

The GPS observations used in this study provide a data set that is unique because it provides dense coverage of the surface displacements at intermediate and large scale. Publicly available GPS data in this region (from the International GPS Service) are limited to only 3 stations at large distances from the earthquake. Our (SEAMERGES) GPS network comprises 49 continuously operating stations in Indonesia (6), Malaysia (38) and Thailand (5). In addition, data from 7 campaign sites in Thailand, observed in October 2004 and in February 2005, are incorporated in the analysis. Furthermore, the network is extended with 9 regional and 21 global stations of the International GPS Service (IGS). The combined co-seismic displacement field is presented in Fig. 1 (and Supplementary Table 1). Only stations located more than 4,000 km away from the epicentre (for example, KIT3 in Uzbekistan and KARR in Australia) are unaffected by the earthquake. Small, but significant, co-seismic jumps between 5 and 10 mm are detected even at stations more than 3,000 km away from the earthquake epicentre—for example, in southern China (Kunming), continental India (Bangalore, Hyderabad) and eastern Malaysia (Sabah). Even stations at Diego Garcia island in the Indian Ocean and in the Philippines were displaced by more than 5 mm. The nearest sites, more than 400 km away from the epicentre, show very large co-seismic displacements: 27 cm in Phuket, Thailand, 17 cm on Langkawi island, Malaysia, and 15 cm in Sampali, Indonesia.

Overall, the deformation field points inward towards the earthquake epicentre. East–west-trending displacements at mid-latitudes (between 0° and 15°), north–south-trending displacements at higher latitudes (below 0° or above 15°), and absence of significant displacements north (LHAS) and south (BAKO) of the rupture are due to a thrust focal mechanism, aligned with the Sumatran trench west of the west coast of Sumatra. Large displacements in northern Thailand (8 cm in Bangkok and almost 3 cm in Chiang Mai) imply a rupture extending far north into the Andaman Sea, in agreement with the distribution of aftershocks. On the other hand, the very strong increase of displacements detected along the Malaysian

[1]Laboratoire de Géologie, ENS/CNRS, 75231 Paris, France. [2]DEOS, Delft University of Technology, 2629 HS Delft, The Netherlands. [3]Department of Survey and Mapping Malaysia (DSMM), 50578 Kuala Lumpur, Malaysia. [4]Royal Thai Survey Department (RTSD), Bangkok 10200, Thailand. [5]Department of Survey Engineering, Chulalongkorn University, Bangkok 10330, Thailand. [6]Department of Geology, Chulalongkorn University, Bangkok 10330, Thailand. [7]National Coordination Agency for Surveys and Mapping (BAKOSURTANAL), Cibinong 16911, Indonesia. [8]University of Technology Malaysia (UTM), 81310 Johor, Malaysia. [9]Institute of Technology Bandung (ITB), Bandung 40132, Indonesia. †Present address: ESS Department, University of California Los Angeles (UCLA),90095-1567 California, USA.

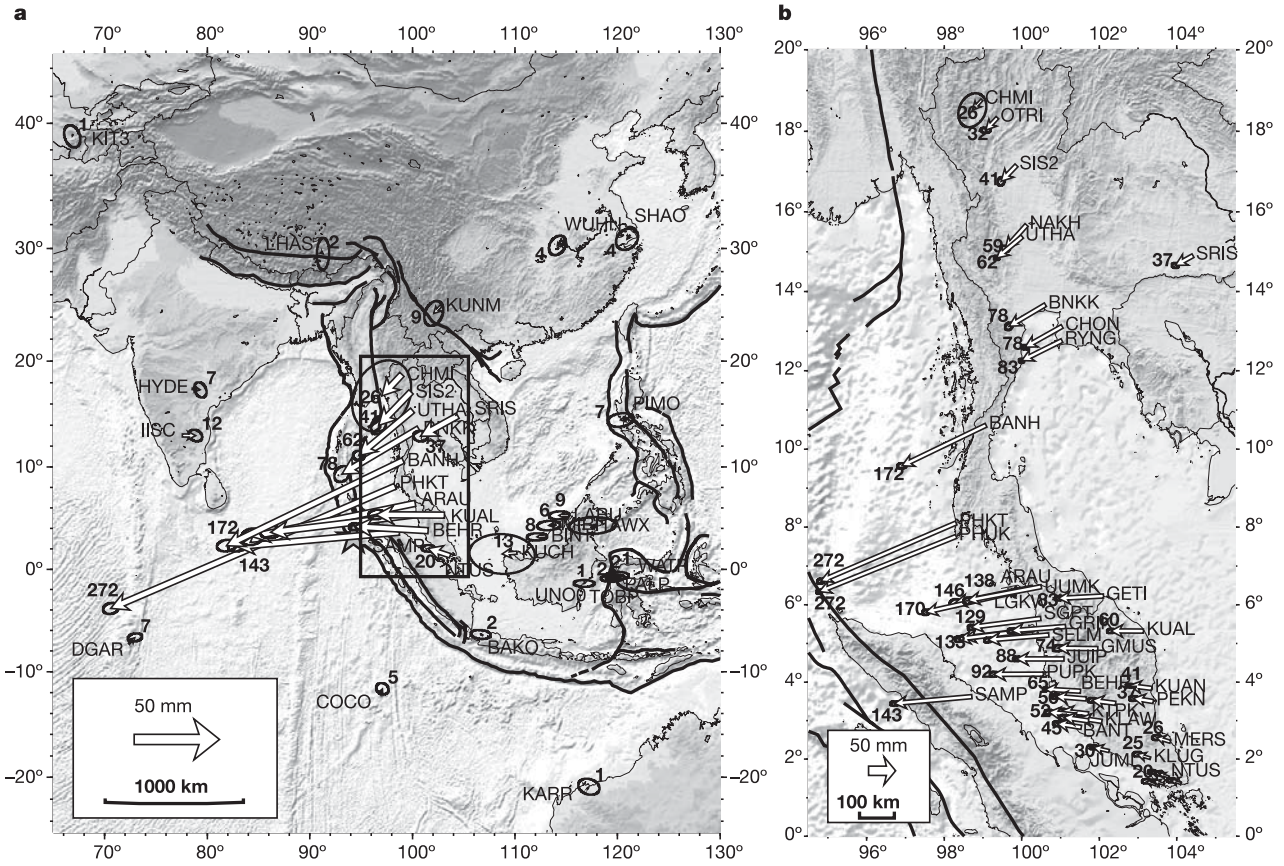

Figure 1 | Co-seismic displacement field derived from GPS observations at more than 60 sites. Panel **a** shows a large scale overview from a low-density subset. Panel **b** provides more detail, zooming in on a smaller area (rectangular box in **a**). Note the high-density sub-network on the Malaysian peninsular. Bold numbers next to arrow heads give the displacement in mm. Ellipses depict the 90% confidence level. Thin black lines depict major faults[8]. The USGS earthquake epicentre location is portrayed by the star symbol, near bottom left of box. ETOPO-5 and GTOPO-30 Digital Elevation Models were used to generate the background topography and bathymetry.

peninsula (2 cm in Singapore, 17 cm in Langkawi island) suggests a limited amount of slip on the southern section of the fault.

Elastic co-seismic modelling

Observed surface displacements are modelled using Okada's formulation of a dislocation buried in an infinite elastic half-space[5]. A first model (model A) was constructed using the USGS[6] and CMT[7] parameters: localization, depth, focal mechanism and magnitude. To match these parameters, we assume a rectangular dislocation plane of 450 km length and 145 km width, dipping with an angle of 8° and emerging at the surface roughly along the trench. Assuming a rigidity coefficient of 4×10^{11} GPa, a uniform slip of 12 m perpendicular to the trench direction gives a total seismic moment of 3×10^{22} N m and a moment magnitude $M_w = 9.0$, in agreement with the CMT value. With an average misfit of 27 mm this model matches well the observed deformation in northern Sumatra

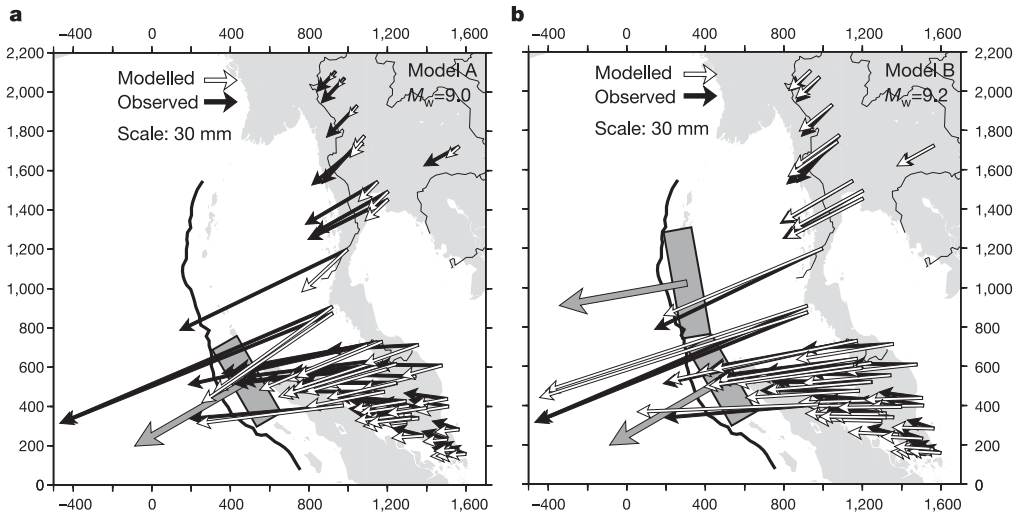

Figure 2 | Elastic modelling of co-seismic deformation. GPS results (black arrows) and model predictions (white arrows) are shown. Grey rectangles depict models for rupture planes buried at depth (see text for details). Grey arrows show the modelled direction and amount of slip. Model A (panel **a**) uses a 450-km-long rupture and model B (panel **b**) uses a 1,000-km-long rupture, curved along the trench in two segments. *x* and *y* axes show distance (km) in a UTM (Universal Transverse Mercator) projection.

(SAMP) and the Malaysian peninsula, but fails to predict the large deformation observed in the northern part of the network (Fig. 2). Only half of the observed deformation (15 cm instead of 27 cm) is predicted at Phuket island (PHKT). Only one-third of the observed deformation (3 cm instead of 8 cm) is predicted at Bangkok (BNKK). Finally, insignificant displacements are predicted further north in China and further west in continental India, which is in contradiction with the observations. Therefore, we can conclude that a much longer rupture must be considered.

A second model (not shown) was then constructed by simply prolonging the rupture plane further north to a total length of 1,000 km. All other parameters were kept identical to those of model A. Although this simple model fails to predict the details of the observed deformation field (in particular, the directions in continental Malaysia), it matches better the observed far-field deformation, both in amplitude and direction, with an average misfit reduced to 12 mm. The corresponding seismic moment is increased to 7×10^{22} N m and the magnitude to $M_w = 9.2$. However, it is very clear that such a rupture plane does not follow the trench direction in this area. The trench is curved to an almost north–south azimuth above a latitude of 5° N. Therefore, we constructed a third model (model B) by simply cutting the previous plane into two planes: the southernmost one with a length of 450 km and the original strike of 330°, and the second one with a length of 550 km and striking 350°. The total length and the slip being identical to those of the previous model, the seismic moment and the magnitude remained unchanged. The better alignment with the trench leads to a better fit with the observed deformation (the average misfit is now reduced to 10 mm), mostly in the predicted deformation direction, as expected (Fig. 2). This is true in particular in the central part of the network, in northern Malaysia and Thailand. As good as it is, this model still predicts too much deformation in the southern part of the Malaysian peninsula. Here, the observed displacements are consistently smaller (by 1 cm on average) than the predicted ones and point more to the north. Reduction of predicted deformation in south Malaysia can only be achieved by reducing the amount of slip on the southern part of the rupture. In fact, a fourth model (not shown)—in which we impose a reduced slip of only 3 m on the first half of the southern plane, balanced by an increased slip on the second half—yields an even better fit, with an average misfit reduced to 8 mm.

In order to investigate the effect of non-homogeneous slip on the fault, we construct a model with a grid of multiple nodes on which we invert the amount of slip, keeping its direction fixed. The surface fault geometry follows the mapping of ref. 8, the dip angle is fixed to 13° according to USGS determination[6], and the maximum depth is 50 km. All models providing a good fit require a very small amount of slip on the southernmost part of the rupture (which starts around Simelue island, Indonesia), a very localized patch of very large slip (>20 m) in front of Phuket, Thailand, and a third patch of slip more spread out further north. All models also require that slip stops

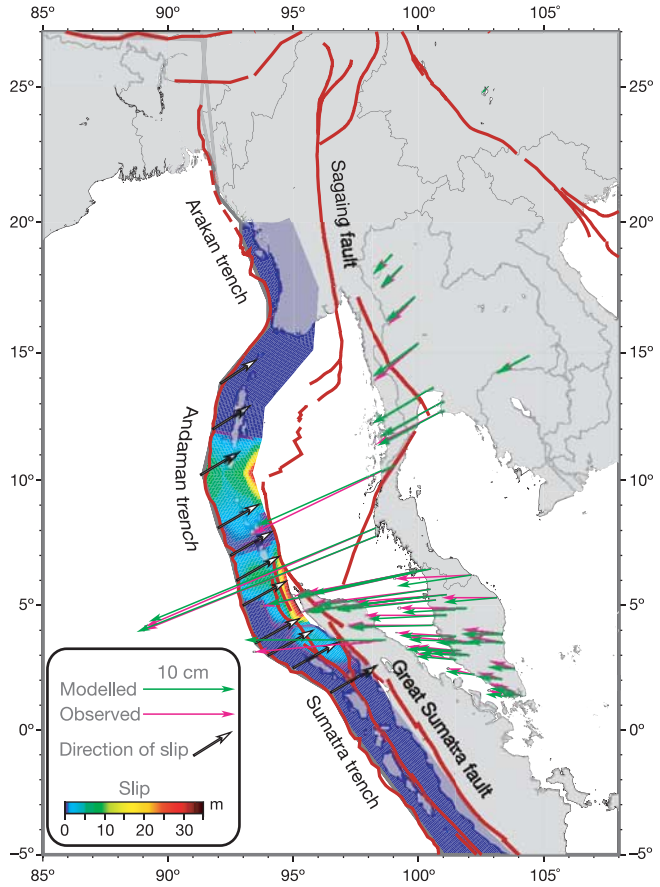

Figure 3 | Best-fit elastic model of the co-seismic displacements using non-homogeneous slip along the rupture plane. Colour code indicates the amount of slip from 0 (dark blue) to 35 m (dark red). Note that the area with significant slip is approximately 1,100 km long. Measured displacements (purple vectors) and modelled deformation (green vectors) are also depicted. Thin red lines depict major faults[8].

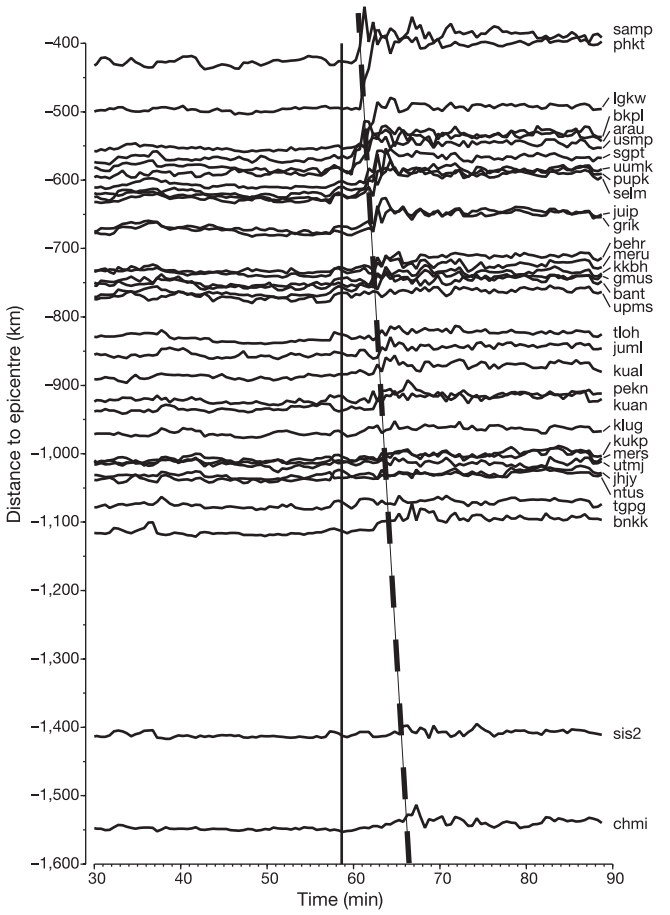

Figure 4 | Kinematic solution of the co-seismic displacements for 33 continuous GPS stations in southeast Asia. Each curve shows the variation in the horizontal position of a given station during 1 h around the time of the earthquake (1 point every 30 s). Curves are sorted by distance to the earthquake epicentre, from 450 km for station SAMP (Medan, northern Sumatra, top) to 1,500 km for station CHMI (Chiang Mai, Thailand, bottom). The vertical full line indicates the time of the earthquake (0 h 59 min) and the second, oblique, dashed line indicates the expected surface wave arrival time assuming a group velocity of 3.6 km s^{-1}.

around 13°–14° latitude, which matches very well the end of the aftershock area[6] and the crucial changes in the bathymetry of the trench in the area[9]. Also, the patch with hardly any slip between 7° and 8° is a feature that persists throughout all our inversions. The best fitting model (Fig. 3) provides a normalized χ^2 of 2.2 and an average misfit of 4 mm. It requires slip to be moderate near the surface and maximum at the bottom of the fault, possibly like the 1881 Nicobar earthquake[10]. Imposing more slip at the surface degrades the fit (χ^2 is increased by 50%), but is still in the range of very plausible solutions: total average misfit is 6 mm. Far-field observed displacements are also matched by our best-fit elastic model. We compute 11 mm (instead of 9 mm) at Kunming, 8 mm at Manilla (instead of 7 mm), 13 mm at Bangalore (instead of 12 mm) and 7 mm (as observed) at Hyderabad. Finally, the model predicts displacements of the order of magnitude of 2–5 m near the fault itself, on the Andaman and Nicobar islands. These values will have to be matched with precise GPS surveys conducted there by Indian institutes.

There is a clear trade-off between the maximum slip and the width of the fault or the depth of the fault on which slip is distributed. Obviously, our deformation field lacks the sensitivity of near-field data to fully resolve this issue. Another limitation of our inversion is the assumed constant azimuth of the slip along the rupture plane. Although this azimuth is a reasonable average, there is a slight misalignment with the aftershocks' slip vector direction at the northern termination of the rupture. Finally, the contrast in elastic parameters east of the trench between continental crust in the south and oceanic lithosphere in the north must probably be taken into account. However, the heterogeneity and localization of slip on the southern half of the rupture is in very good agreement with independent determinations from the inversion of short-period seismic body waves (http://iisee.kenken.go.jp/staff/yagi/eq/Sumatra2004/Sumatra2004.html). The corresponding seismic moment and magnitude that we compute depends on the assumed rigidity coefficient. Obviously, the GPS data we present here constrain well the length of the rupture, give some insight on the slip × fault width product, but give no information at all on the rigidity. However, our magnitude of 9.2 matches well the determination of 9.3 inferred using the longest-period normal mode of the Earth over a longer time period than CMT determination[11], even if this latter determination has been slightly overestimated because of the neglect of self-gravitational effects.

Kinematic positioning

Although only measurements averaged over 24 h give the ultimate precision of a few millimetres that are expected from GPS, it is also possible to compute each station position on an epoch-by-epoch basis, that is, at the sampling rate of the GPS signal at each station (30 s in this case). GPS stations start to move when surface waves emitted by the hypocentre hit their location, then within minutes they stabilize to their new position (Fig. 4). Knowing surface wave velocity, it is straightforward to predict 'arrival times' at each station and to match them to the 'jumps' in the time series. GPS records are equivalent to very-low-frequency seismograms, so that they can be used to determine the position of the centroid of deformation at the origin of the bulk of the surface wave emission. In this case, to sort arrival times, we need to move the source of the bulk of the signal almost 200 km north of the USGS-determined epicentre. This corresponds very well to the patch of high slip already determined from our co-seismic static displacements. In addition, it can be seen that stations north of the epicentre reach their final position not only later but also slower than stations in the south. Stations PHKT, SAMP or LGKW have rise times of 1 or 2 min, whereas BNKK and CHMI take up to 5 min to rise. This is due to the slow northward propagation of the rupture along the trench after the initial rupture. Phuket's initial motion (around 2 min 39 s after the earthquake time

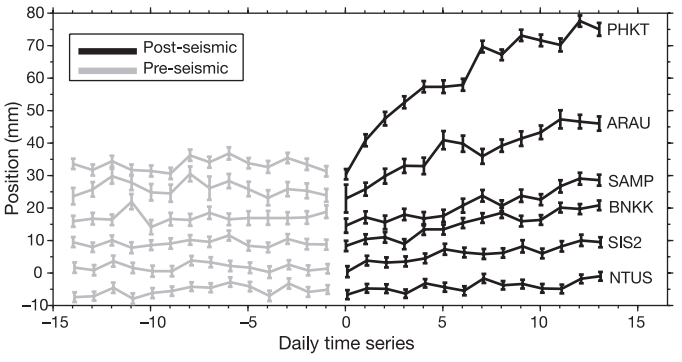

Figure 5 | Pre- and post-seismic position variations derived from GPS observations at selected stations. Daily solutions and 1σ uncertainties are depicted before the earthquake (grey lines) and after the earthquake (black lines) Note the scale is in mm. Initial position is arbitrary, and co-seismic jump is removed.

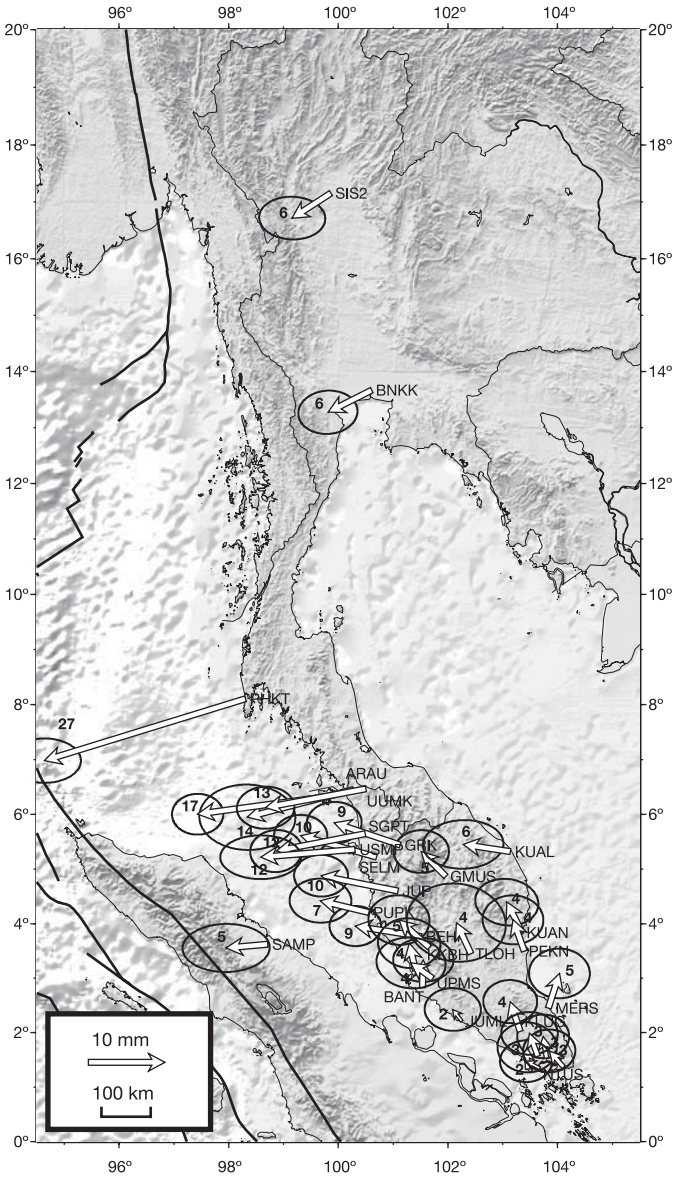

Figure 6 | Five-day post-seismic displacement field. Bold numbers next to arrow heads give the displacement in mm. Ellipses depict the 90% confidence level. Black lines depict major faults[8]. ETOPO-5 and GTOPO-30 Digital Elevation Models were used to generate the background topography and bathymetry.

tag) is towards the south-southwest, in the direction of the point where the rupture started. Three minutes later, the point stops moving and the displacement vector points towards the west-southwest, where the first rupture ended. During this elapsed time, the rupture travelled through a distance of approximately 650 km, yielding a velocity of 3.7 km s^{-1}. The second half of the rupture is slightly smaller (450 km) and is covered in around 4 min. This yields a slower rupture velocity of around 2 km s^{-1}. (A GIF animation is available; see Supplementary Information.)

Given the sampling rate of 30 s of the GPS signal, the uncertainty can be roughly estimated at ± 0.5 km s^{-1}. Therefore, it can be concluded that the second part of the rupture is significantly slower than the first part. Nevertheless, the fact that the northernmost stations reached their final position less than 10 min after the earthquake rules out the possibility of a completely silent aseismic rupture (that is, with a period $>$600 s).

Post-seismic deformation

Post-seismic deformation results from a combination of different phenomena, each of which has a characteristic timescale. Deformation occurring over a period of a month represents mostly immediate after-slip, due to either aseismic slip in the poorly consolidated sediment layer overlying the fault or co-seismic slip associated with the aftershock sequences. Deformation occurring over a period of a year might be dominated by poro-elasticity, and thereafter by visco-elastic or plastic flow from low-viscosity shallow earth layers. An increasing amount of evidence indicates that after-slip follows the majority of earthquakes, particularly in subduction zones[12–14]. Here also, post-seismic motions started right after the co-seismic elastic displacements (Fig. 5). Additional displacements of up to 4 cm over a 15 d period after the earthquake are detected at the nearest station (PHKT). Here, the apparent logarithmic decay suggests aseismic slip in a shallow layer rather than cumulated aftershock-induced slip which should follow the well known hyperbolic trend (Omori's law)[15]. The pattern of after-slip cumulated 5 d after the earthquake is also more probably due to aseismic slip (Fig. 6 and Supplementary Table 2). After-slip is maximum at PHKT (3 cm) and in the same direction as co-seismic slip. The along-trench orientation of the observed vectors in south Malaysia is difficult to model with an elastic dislocation. However, the rest of the vectors point to the same patches of high slip that were identified in the co-seismic section. Finally, relative to co-seismic slip, after-slip seems to be proportionally more important in the northern section of the rupture than in the south.

Post-seismic motions continue, and will continue for a long period of time. Fifty days after the earthquake, the island of Phuket had already moved 34 cm, which is 1.25 times the initial co-seismic displacement.

Seismic hazard in southeast Asia

An earthquake on the Sumatran trench was not unexpected. In the Sumatran subduction zone, convergence normal to the trench occurs at 4–5 cm yr^{-1}. Even near its boundaries, internal deformation of the Sundaland plate is generally small ($<$3 mm yr^{-1})[16]. North Sumatra was a notable exception, as both local and regional GPS networks there detected significant deformation hundreds of kilometres away from the trench[2,16]. This deformation was interpreted as accumulation of elastic deformation over a wide area, indicating 'high coupling' with subduction. This is in contrast with south Sumatra (south of Enggano island, approximately 3° S) and Java, where inter-seismic deformation is less intense, which is probably related to the variable dip angle and changing obliquity of the subduction. However, because it ruptured only a segment of the subduction zone, the earthquake increased stress on adjacent segments, further south on the Sumatran trench[17], but also further north on the Arakan trench in Myanmar. The M_w 8.7, 28 March earthquake is a first consequence of that. In addition, strain favouring future rupture has probably been added on the strike-slip system behind the subduction: the Great Sumatran fault in Sumatra and the Sagaing fault in Myanmar. Along-strike additional strain depends on the precise orientation of the rupture: essentially zero if exactly perpendicular to the strike-slip system, it will be increased if oriented north of this azimuth, and decreased if oriented south. In all cases, normal strain will be applied to these faults, favouring unclamping and easing slip. Because historical major earthquakes on these faults have proved that they release strain in a seismic mode[18,19], the probability of large earthquakes on these structures in the near future is very high.

Finally, stress transfer has been shown to potentially trigger earthquakes on surrounding faults[20]. This stress transfer can be instantaneous (Coulomb stress failure) or delayed in time if associated with fluid migration in the brittle crust, and this is particularly true for the unclamping effect[21]. Should this effect play an important role, the foreseen time delay could be of the order of magnitude of a year. Therefore, post-seismic measurements (by GPS stations installed after the earthquake) monitoring the surface deformation for the years to come will provide crucial information on the earthquake mechanism and on possible follow-on scenarios.

METHODS

Static positioning. The data are processed with the GIPSY-OASIS II software, using the (optimized) Precise Point Positioning (PPP) methodology[22], including ambiguity resolution for the entire network. For the continuously operating stations, this results in a set of independent daily network solutions, covering a period from 14 d before to 14 d after the earthquake. These daily solutions are subsequently combined into two campaign-like averaged solutions (before and after the earthquake). Next, the pre-earthquake solution is mapped onto the International Terrestrial Reference Frame (ITRF) 2000[23], using a subset of 14 well-determined IGS global reference stations with a smooth positioning history. This is done to establish an undeformed reference solution, which is not affected by episodic jumps in the time series of some of the IGS stations. The post-earthquake solution is then projected on this reference solution using only those stations that are unaffected by co-seismic motions. The co-seismic displacements of the stations in the earthquake region then simply follow from coordinate differences between the two solutions, with a relative (2σ) accuracy of about 2 mm. The GPS campaign data of the 7 additional sites in Thailand are treated in a slightly different way to compensate for the larger time difference between the two campaigns (4 months) and to remove the effects of post-seismic deformation. This is done by removing the long-term rigid plate motions predicted at these locations according to the latest geodetic models[16] and by correcting the total displacements with an estimation of the post-seismic motions based on the results of nearby permanent stations. For the 7 additional Thailand sites a differential horizontal positioning (2σ) accuracy of 6 mm is achieved.

Kinematic positioning. In this approach, absolute station position are computed every 30 s with the GIPSY PPP methodology by using high-rate GPS satellite clock solutions. Each point has a higher uncertainty and is affected by biases which usually cancel out over long periods of measurement. However, the co-seismic signal is clearly detectable in these data: stations within a range of 1,500 km from the earthquake epicentre show displacements up to 3 cm, which is significantly higher than the high-frequency noise of around 1 cm typically obtained in kinematic positioning.

Elastic modelling. Forward models (Fig. 2a, b) are computed with RNGCHN software[24]. The average misfit of a given model is simply the sum of the residual displacements (difference between observed and modelled displacements) at each station, divided by the number of stations.

Inverse models are computed with DEFNODE software (http://www.rpi.edu/~mccafr/defnode; refs 25, 26). The inversion gets the parameters that minimizes the reduced χ^2 statistic: $\chi^2_n = \sqrt{\sum r^2/s^2}/\mathrm{dof}$, where r is the residual, s is the standard deviation and dof is the degree of freedom. Minimization is performed using the downhill simplex technique.

Received 17 March; accepted 16 June 2005.

1. Michel, G. W. *et al.* Crustal motion and block behaviour in SE-Asia from GPS measurements. *Earth Planet. Sci. Lett.* **187**, 239–244 (2001).
2. Bock, Y. *et al.* Crustal motion in Indonesia from GPS measurements. *J. Geophys. Res.* **108**, doi:10.1029/2001JB000324 (2003).

3. Socquet, A. *et al.* Indian plate motion and deformation induced along its boundary with Sunda in Myanmar determined by GPS. *J. Geophys. Res.* (submitted).
4. Prawirodirdjo, L. *et al.* Geodetic observations of interseismic strain segmentation at the Sumatra subduction zone. *Geophys. Res. Lett.* **24,** 2601–2604 (1997).
5. Okada, Y. Surface deformation due to shear and tensile faults in a half-space. *Bull. Seismol. Soc. Am.* **75,** 1135–1154 (1985).
6. USGS fast moment tensor solution. ⟨http://wwwneic.cr.usgs.gov/neis/eq_depot/2004/eq_041226/neic_slav_q.html⟩.
7. Harvard moment tensor solution. ⟨http://wwwneic.cr.usgs.gov/neis/eq_depot/2004/eq_041226/neic_slav_hrv.html⟩.
8. Pubellier, M., Ego, F., Chamot-Rooke, N. & Rangin, C. The building of pericratonic mountain ranges: structural and kinematic constraints applied to GIS-based reconstructions of SE Asia. *Bull. Soc. Geol. Fr.* **174,** 561–584 (2003).
9. Nielsen, C., Chamot-Rooke, N., Rangin, C. & the Andaman cruise team, From partial to full strain partitioning along the Indo-Burmese hyper-oblique subduction. *Mar. Geol.* **209,** 303–327 (2004).
10. Ortiz, M. & Bilham, R. Source area and rupture parameters of the 31 December Mw = 7.9 Car Nicobar earthquake estimated from tsunamis recorded in the Bay of Bengal. *J. Geophys. Res.* **108,** doi:10.1029/2002JB001941 (2003).
11. Stein, S. & Okal, E. Speed and size of the Sumatra earthquake. *Nature* **434,** 581–582 (2005).
12. Heki, K., Miyazaki, S. & Tsuji, H. Silent fault slip following an interplate thrust earthquake at the Japan Trench. *Nature* **386,** 595–597 (1997).
13. Ruegg, J. C., Olcay, M., Armijo, R., DeChabalier, J. B. & Lazo, D. Coseismic and aseismic slip observed from continuous GPS measurements for the 2001 Southern Peru Earthquake (Mw = 8.4). *Seismol. Res. Lett.* **72,** 680–685 (2001).
14. Marquez-Azua, B., DeMets, C. & Masterlark, T. Strong interseismic coupling, fault afterslip, and viscoelastic flow before and after the Oct. 9, 1995 Colima-Jalisco earthquake: Continuous GPS measurements from Colima, Mexico. *Geophys. Res. Lett.* **29,** doi:10.1029/2002GL014702 (2002).
15. Scholz, C. Earthquakes and friction laws. *Nature* **391,** 37–42 (1998).
16. Simons, W. *et al.* A decade of GPS measurements in SE Asia: (Re)Defining Sundaland motion and its boundaries. *J. Geophys. Res.* (submitted).
17. McCloskey, J., Nalbant, S. S. & Steacy, S. Earthquake risk from co-seismic stress. *Nature* **434,** 291 (2005).
18. Sieh, K. & Natawidjaja, D. Neotectonics of the Sumatran fault. *J. Geophys. Res.* **105,** 28295–28326 (2000).
19. LeDain, A. Y., Tapponnier, P. & Molnar, P. Active faulting and tectonics of Burma and surrounding regions. *J. Geophys. Res.* **89,** 453–472 (1984).
20. Stein, R. S. The role of stress transfer in earthquake occurrence. *Nature* **402,** 605–609 (1999).
21. Vigny, C. *et al.* Migration of seismicity and earthquake interactions monitored by GPS in SE Asia triple junction: Sulawesi, Indonesia. *J. Geophys. Res.* **107,** doi:10.1029/2001JB000377 (2002).
22. Zumberge, J. M., Heflin, M., Jefferson, D., Watkins, M. & Webb, F. Precise point positioning for the efficient and robust analysis of GPS data from large networks. *J. Geophys. Res.* **102,** 5005–5017 (1997).
23. Altamimi, Z., Sillard, P. & Boucher, C. ITRF 2000: A new release of the International Terrestrial Reference frame for earth science applications. *J. Geophys. Res.* **107,** doi:10.1029/2001JB000561 (2002).
24. Feigl, K. & Dupré, E. RNGCHN: A program to calculate displacement components from dislocations in an elastic half-space with applications for modelling geodetic measurements of crustal deformation. *Comput. Geosci.* **25,** 695–704 (1999).
25. McCaffrey, R. in *Plate Boundary Zones* (eds Stein, S. & Freymueller, J.) 101–122 (Geodynamics Series 30, American Geophysical Union, Washington DC, 2002).
26. McCaffrey, R. Block kinematics of the Pacific–North America plate boundary in the southwestern US from inversion of GPS, seismological, and geological data. *J. Geophys. Res.*(in the press).

Supplementary Information is linked to the online version of the paper at www.nature.com/nature.

Acknowledgements Thanks are extended to the different national agencies (DSMM, RTSD, BAKOSURTANAL) for sharing their regional GPS data in the framework of the SEAMERGES (http://www.deos.tudelft.nl/seamerges) project. We also thank M. Hashizume for contributing Thai data collected by Chulalongkorn University in cooperation with the 'Frontier Observational Research System for Global Change' (FRONTIER) project and the Earthquake Research Institute at the University of Tokyo; and we thank the Dutch research programme Integrated Solid Earth Science (ISES), the French Institut National des Sciences de l'Univers (INSU-CNRS) and the French ministry of foreign affairs (MAE) for providing equipment and financial support. Our sympathy is extended to the relatives of the Phuket GPS station operator who is still reported missing after the tsunami disaster. SEAMERGES has been funded by the ASEAN-EU University Network Programme (AUNP). The contents of this paper are the sole responsibility of the authors listed and cannot be regarded as reflecting the position of the European Union.

Author Information Reprints and permissions information is available at npg.nature.com/reprintsandpermissions. The authors declare no competing financial interests. Correspondence and requests for materials should be addressed to C.V. (vigny@geologie.ens.fr).